Spatial and Temporal Distribution of Driving Rain on Buildings: Numerical Simulation and Experimental Verification

Bert Blocken **Jan Carmeliet, Ph.D.**

ABSTRACT

This paper presents a review and application results of a practical numerical method to determine both the spatial and temporal distribution of driving rain on buildings. It is based on an existing numerical simulation technique and uses the building geometry and climatic data at the building site as input. The method is applied to determine the three-dimensional spatial and temporal distribution of driving rain on a low-rise building of complex geometry for an on-site recorded rain event. Distinct wetting patterns are found, the features of which are analyzed. The comparison of the numerical results with full-scale measurements shows good agreement. The importance of time representativeness of climatic input data for the numerical method is emphasized. For this purpose, a new weighted averaging technique for wind and rain data is presented.

INTRODUCTION

Driving rain is one of the most important moisture sources affecting building envelopes. Information concerning the exposure to driving rain is essential to design building envelopes with satisfactory hygrothermal performance and is an essential requirement as a boundary condition for heat-air-moisture (HAM) transfer analysis. Until recently, research on driving rain has mainly been limited to field experiments and the use of empirical formulae. As research efforts continued to reveal the inherent complexity of the problem, researchers realized that further achievements were to be found through numerical analyses.

In the past ten years, the introduction of computational fluid dynamics (CFD) in the area has provided new insights in the interaction between wind, rain, and the building envelope. Choi (1991) developed a numerical simulation technique to determine the distribution of driving rain on buildings under steady-state conditions of wind and rain. This publication and the following contributions based on this technique considerably extended the existing knowledge (Choi 1993, 1994a, 1994b; Wisse 1994; Sankaran and Paterson 1995; Lakehal et al. 1995; Karagiozis and Hadjisophocleous 1996; Karagiozis et al. 1997; van Mook et al. 1997; van Mook 1999a, 1999b; Hangan 1999; Etyemezian et al. 2000; Blocken and Carmeliet 2000a, 2000b).

Until now, only a few attempts have been made for experimental verification (Lakehal et al. 1995; van Mook 1999a, 1999b; Hangan 1999). These research efforts focused on single stationary rain events (i.e., single intervals with a stationary value of wind speed, wind direction, and rainfall intensity). A numerical method for estimating transient driving rain loads was introduced by Blocken and Carmeliet (2000a, 2000b). At that time, a preliminary two-dimensional experimental verification was conducted. Important topics to be explored next are a more extensive experimental verification of the numerical method for transient rain events and the study of driving rain on buildings of complex geometry. Attention should also be given to the sampling requirements to which wind and rain data for driving rain estimation should adhere. These issues are the subject of this paper.

SPECIFIC CATCH RATIO AND CATCH RATIO

In the past, different terms have been used by different researchers to describe the quantity of driving rain. The terms

Bert Blocken is a Ph.D. student and **Jan Carmeliet** is a professor at the Laboratory of Building Physics, Department of Civil Engineering, Katholieke Universiteit, Leuven, Belgium.

used by the current authors (specific catch ratio and catch ratio) are based on the work by Van Mook et al. (1997) and Bollen and Eerdekens (1998). The specific catch ratio and catch ratio, respectively, are equal to the LEF (local effect factor) and LIF (local intensity factor) used by Choi (1993). The specific catch ratio η_d (for one raindrop diameter d) is defined as

$$\eta_d(t) = \frac{R_{dr}(d, t)}{R_h(d, t)} \quad (1)$$

where

$R_{dr}(d, t)$ = driving rain intensity for raindrop diameter d at time t,

$R_h(d, t)$ = horizontal rainfall intensity (i.e., the rainfall intensity through a horizontal plane) for raindrop diameter d at time t,

and the catch ratio η (integrated over all raindrop diameters),

$$\eta(t) = \frac{R_{dr}(t)}{R_h(t)} \quad (2)$$

where

$R_{dr}(t)$ = the driving rain intensity (for all raindrop diameters) at time t,

$R_h(t)$ = horizontal rainfall intensity (for all raindrop diameters) at time t.

The catch ratio will generally be measured and calculated for discrete time steps $[t_j, t_j+\Delta t]$ and is then redefined as

$$\eta(t_j) = \frac{\int_{t_j}^{t_j+\Delta t} R_{dr}(t)dt}{\int_{t_j}^{t_j+\Delta t} R_h(t)dt} = \frac{S_{dr}(t_j)}{S_h(t_j)} \quad (3)$$

where

$S_{dr}(tj)$ = driving rain amount during time step $[t_j, t_j+\Delta t]$,

$S_h(tj)$ = the horizontal rainfall amount during time step $[t_j, t_j+\Delta t]$.

The six basic influencing parameters for the catch ratio as defined in Equation 3 are (1) building geometry (including environment topology), (2) position on the building envelope, (3) wind speed U, (4) wind direction ϕ, (5) horizontal rainfall intensity R_h, and (6) raindrop size distribution f_h. The turbulent dispersion of raindrops is neglected in the present study.

NUMERICAL METHOD: A REVIEW

Steady-State Simulation Technique

The simulation technique developed by Choi (1991, 1993, 1994a) comprises the following four steps: (1) calculating the steady-state wind flow pattern around the building using a CFD code, (2) obtaining raindrop trajectories in the flow pattern, (3) determining the specific catch ratio from the configuration of the raindrop trajectories, and (4) calculating the catch ratio based on the specific catch ratio and the raindrop spectrum. This procedure yields the driving rain amount at a certain building envelope position under steady-state conditions of wind and rain.

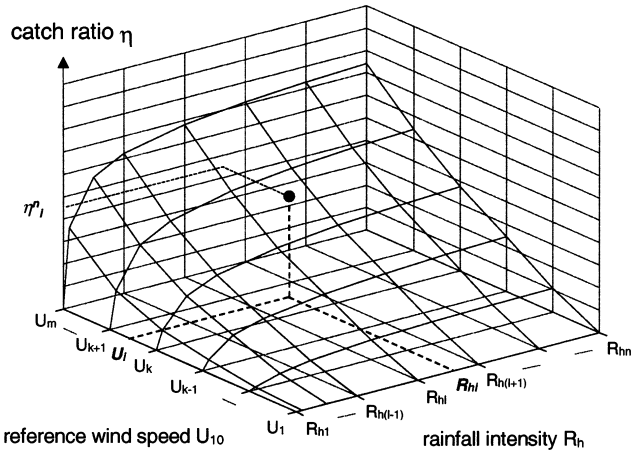

Figure 1 *Example graph of the catch ratio as a function of wind speed and rainfall intensity (for a given wind direction and a given position on the building envelope).*

Method for Transient Rain Events

The numerical method for transient driving rain loads (Blocken and Carmeliet 2000a, 2000b) is an extension of Choi's steady-state simulation technique into the time domain and uses climatic data records (wind speed, wind direction, rainfall intensity) at the building site as input. In the interest of brevity, we will not go into the details of this method. Only an outline will be given here. Let a series of steady-state simulations (four-step technique by Choi) be conducted for different values of wind speed, direction, rainfall intensity, and various positions on the building envelope. From these simulations, we construct surface plots such as that given in Figure 1. Each of these plots displays the catch ratio as a function of wind speed and rainfall intensity for one specific building envelope position and one wind direction value. In constructing these plots, we adopt the raindrop spectrum of Best (1950), linking together raindrop spectrum and rainfall intensity. This way, all six influencing parameters of the catch ratio—mentioned before—are taken into account. To determine the driving rain load for a transient rain event, this event is partitioned into a number of equidistant time steps. Each time step is considered steady state and the climatic data in each time step are used to extract the corresponding catch ratio from the correct plot. An essential part of this method is obtaining representative climatic data (to be explained later). More information can be found in (Blocken and Carmeliet 2000a, 2000b).

APPLICATION AND FULL-SCALE EXPERIMENTAL VERIFICATION

Experimental Facility

The method is applied to determine the spatial and temporal distribution of driving rain on the facade of the low-rise VLIET test building in Heverlee, Leuven. This building was chosen because of its rather complex geometry, allowing a demonstration of the effects of different geometrical configurations and details. It consists of two main modules—the flat roof module, or module 1, and the sloped roof module, or module 2 (Figure 2). There is a small terrace module in between the main modules. The building is 82.7 ft (25.2 m) long and 23.6 ft (7.2 m) wide. The height of the ridges of modules 1 and 2 is 14.1 ft (4.3 m) and 25.9 ft (7.9 m), respectively. The terrace height is 13.0 ft (3.95 m). Roof overhang length varies along the length axis of the building as indicated in Figure 2. The roof overhang for module 1 is 10.6 in. (0.27 m). For module 2, the roof overhang decreases from left to right as indicated in Figure 2: 20.5 – 15.7 – 10.6 in. (0.52 – 0.40 – 0.27 m). The terrace has zero roof overhang. The direction of the prevailing winds at the test site is southwest. Meteorological data are gathered on site by an automatic weather station on a 10-minute basis. In addition, nine driving rain gauges (11.8 by 11.8 $in.^2$ catch area) (0.3 by 0.3 m^2) are positioned on the building envelope (Figure 2). The collected amount of driving rain in gauges 1-6 and 8-9 is measured manually on a daily basis. Gauge 7 is connected to a tipping bucket rain gauge measuring on a 10-minute basis to give more detailed temporal information.

Steady-State Numerical Simulations

Steady-state simulations (following the four-step technique) are conducted for the wind direction perpendicular to the southwest facade, for positions covering the entire southwest facade area, and for a series of wind speed and rainfall intensity values. The simulations provide the data necessary to construct surface plots as given in Figure 1. They include the calculation of the wind flow pattern, the raindrop trajectories, the specific catch ratio, and the catch ratio.

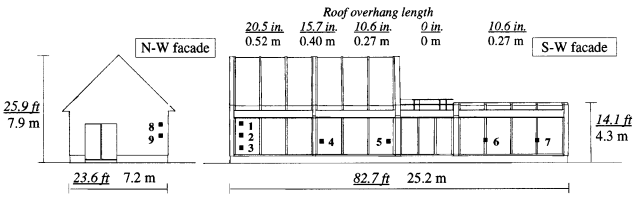

Figure 2 *VLIET test building, northwest and southwest facade, and building dimensions, positions, and numbers of the driving rain gauges (1-9).*

Wind Flow Pattern. The inflow profile for the simulations is based on measurements of the on-site upstream wind speed profile at 6.6, 13.1, 19.7, and 32.8 ft in height (2, 4, 6, and 10 m). The wind simulations are performed on an unstructured, tetrahedral grid with 906,506 cells in a 218.7 × 98.4 × 43.7 yd^3 (200 × 90 × 40 m^3) computational domain using a commercial CFD code. The realizable k-ε turbulence model is used in combination with nonequilibrium wall functions (Shih et al. 1995; Kim et al. 1997). The steady-state wind flow pattern is calculated for reference wind speed U_{10} = 3.3, 6.6, 9.8, 13.1, 16.4, 19.7, 23.0, 26.2, 29.5, 32.8 ft/s (1, 2, 3, 4, 5, 6, 7, 8, 9, 10 m/s) (U_{10} = wind speed at 10 m height).

Raindrop Trajectories. For each of the wind flow patterns calculated, three-dimensional Lagrangian particle tracking is performed for raindrops with 33 different diameters ranging from 0.012 in. (0.3 mm) to 0.039 in. (1 mm) in steps of 0.004 in. (0.1 mm) and from 0.039 in. (1 mm) to 0.236 in. (6 mm) in steps of 0.008 in. (0.2 mm). Figures 3a and 3b show a perspective, front and top views of trajectories of 0.039 in. (1 mm) raindrops in the 16.4 ft/s (5 m/s) and 32.8 ft/s (10 m/s) flow field. In general, it is observed that the inclination of the trajectories and their distortion near the building is more pronounced at higher wind speed. In particular, the following three effects are identified, the first and the second of which are caused by local wind acceleration and are most pronounced at higher wind speed: (1) sweeping of raindrops towards the vertical edges of the facade, (2) sweeping of raindrops towards the upper part of the facade (at the flat roof module and terrace), and (3) shelter provided by roof overhang, limiting the influence of the second effect. Based on these observations, one can expect the spatial distribution to show higher driving rain amounts at the top and side edges of the building than, for example, in the middle of the facade near the ground.

Specific Catch Ratio. The southwest building facade is divided into 40320 square zones of approximately 1.97 × 1.97 $in.^2$ (0.05 × 0.05 m^2). The specific catch ratio is calculated for each zone, for all 33 raindrop diameters, and for each wind speed value. The need for this large amount

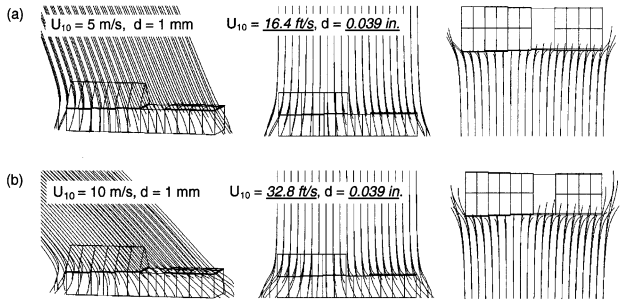

Figure 3 *Perspective, front and top view of raindrop trajectories for* d *= 0.039 in. (1 mm): (a)* U_{10} *= 16.4 ft/s (5 m/s) and (b)* U_{10} *= 32.8 ft/s (10 m/s).*

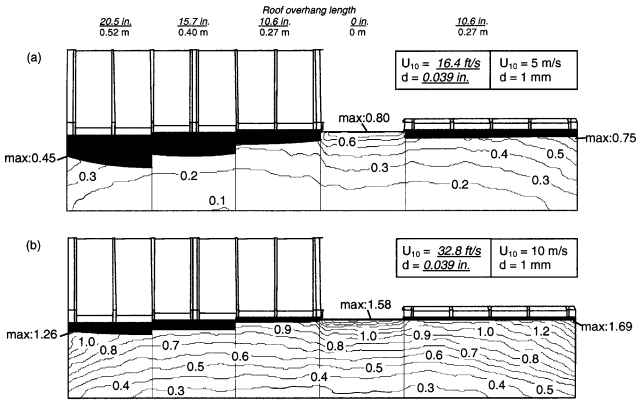

Figure 4 *Contours (numerical) of specific catch ratio at the southwest facade for* d *= 0.039 in. (1 mm): (a)* U_{10} *= 16.4 ft/s (5 m/s) and (b)* U_{10} *= 32.8 ft/s (10 m/s).*

of very small zones was driven by the wish for a high spatial resolution to accurately predict the line on the facade abruptly separating sheltered and nonsheltered facade areas (roof overhang). The spatial variation of the specific catch ratio is presented in Figures 4a and 4b for d = 0.039 in. (1 mm) and U_{10} = 16.4 ft/s (5 m/s) and 32.8 ft/s (10 m/s). Zones sheltered from rain are colored black. The maximum values for each module are indicated. The following observations are made:

1. Shelter by roof overhang evidently increases as the overhang length increases. Near the vertical edges of the sloped roof module, the sweeping effect of drops, both sideward and upward, diminishes the shelter effect, and the line separating sheltered and nonsheltered area (shelter line) shows an upward curvature. At the roof edge of the terrace, the absence of shelter gives rise to high specific catch ratio values.
2. Shelter by roof overhang decreases as wind speed increases, as the trajectories are more inclined and the sweeping effect becomes more important.
3. The spatial uniformity of driving rain on the facade decreases as the wind speed increases. This is clearly shown by the number of contour lines displayed in each figure.
4. In general, the specific catch ratio is larger at the facade of the flat roof and terrace module than at the facade of the sloped roof module. This is caused by the wind blocking effect, which is larger for the latter as was also shown in (Blocken and Carmeliet 2000a).
5. The sweeping effect, both sideward and upward, causes the specific catch ratio to significantly increase toward the vertical building edges and from the lower to the upper part of the facade. The highest values occur at the top and side edges and, if roof overhang is present, just below the abrupt transition from sheltered to nonsheltered area.

Zooming into two selected positions at the facade (positions 4 and 6, corresponding to the positions of the driving rain gauges, see Figure 2), the dependency of the specific catch ratio on wind speed and raindrop diameter is represented in Figures 5a and 5b. It is noted that "position" refers here to the 11.8 × 11.8 in.^{2} (0.3 × 0.3 m^2) area of the driving rain gauge and thus comprises 36 small 1.97 × 1.97 in.^{2} **(**0.05 × 0.05 m^2) zones. Figure 5 displays a significant increase of the specific catch ratio with increasing wind speed and shows a steep increase for small diameters and high wind speed. The effect of roof overhang for position 4 is noticed as a cutoff for U_{10} < 6.5 ft/s (2 m/s). For position 6, shelter is less pronounced as roof overhang length is only 0.27 m here.

Catch Ratio. The catch ratio is obtained by integrating the specific catch ratio over all diameters, taking into account the raindrop spectrum, yielding surface plots of the type given in Figure 1. The plots for position 4 and 6 are presented in Figures 6a and 6b. The effect of wind speed and roof overhang is noticed. The effect of rainfall intensity (and, hence, also of the raindrop spectrum that was taken to be linked with rainfall intensity [Best 1950]) is rather small for rainfall intensities R_h > 0.12 in./h (3 mm/h).

Rain Event

The numerical method is applied for the rain event recorded during January 5 and 6, 1998 (Figure 7). Wind direction during the rain event was in good approximation, perpendicular to the southwest facade (225° from north). Measurements were made of the driving rain amounts during and at the end of the rain event. Studies on driving rain measurement accuracy were recently conducted by Kragh (1998), van Mook (1998), Högberg et al. (1999), and Blocken et al. (2001). The error in driving rain measurements depends on the type of gauge used and on type, duration, and intensity of the spell. Errors for the present rain event are given below.

Temporal Distribution of Driving Rain

The temporal distribution of driving rain is studied by focusing on gauge position 7 (Figure 2). The numerical method for transient rain events described earlier is employed. Using the 10-minute values of wind speed and rainfall intensity (Figure 7), in combination with the surface plot for position 7, 10-minute catch ratio values and driving rain amounts are obtained. Summing these amounts, the cumulative driving rain amount (in., mm) during the rain event is determined (Figure 8). Based on the findings in Blocken et al. (2001), the measurement error for the driving rain amount at the end of the rain event is 0.012 in. (0.3 mm). Compared with Figure 7, it is shown that the largest 10-minute driving rain amounts occur during the co-occurrence of higher wind speed and peak rainfall intensity values. The comparison with the measurements shows a good agreement, although a small underestimation by the numerical method is to be noted. It is also noted that due to the limited resolution of the tipping bucket registration system (0.0044 in./tip or 0.113 mm/tip), only amounts that are

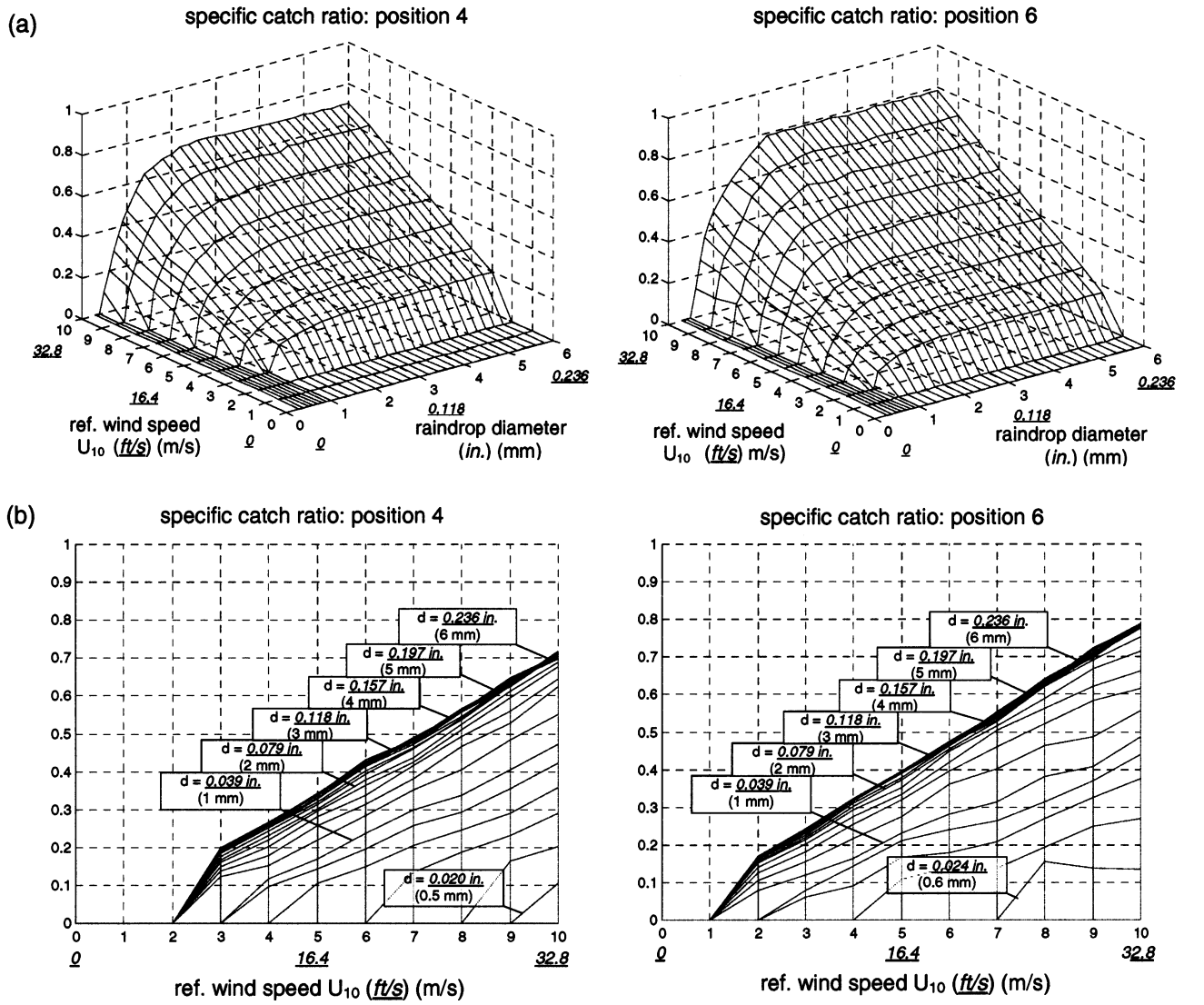

Figure 5 *Specific catch ratio (numerical) as a function of wind speed* U_{10} *and raindrop diameter* d *for position 4 (left figure) and position 6 (right figure) at the southwest facade. (a) Three-dimensional plot and (b) two-dimensional plot with raindrop diameter as a parameter.*

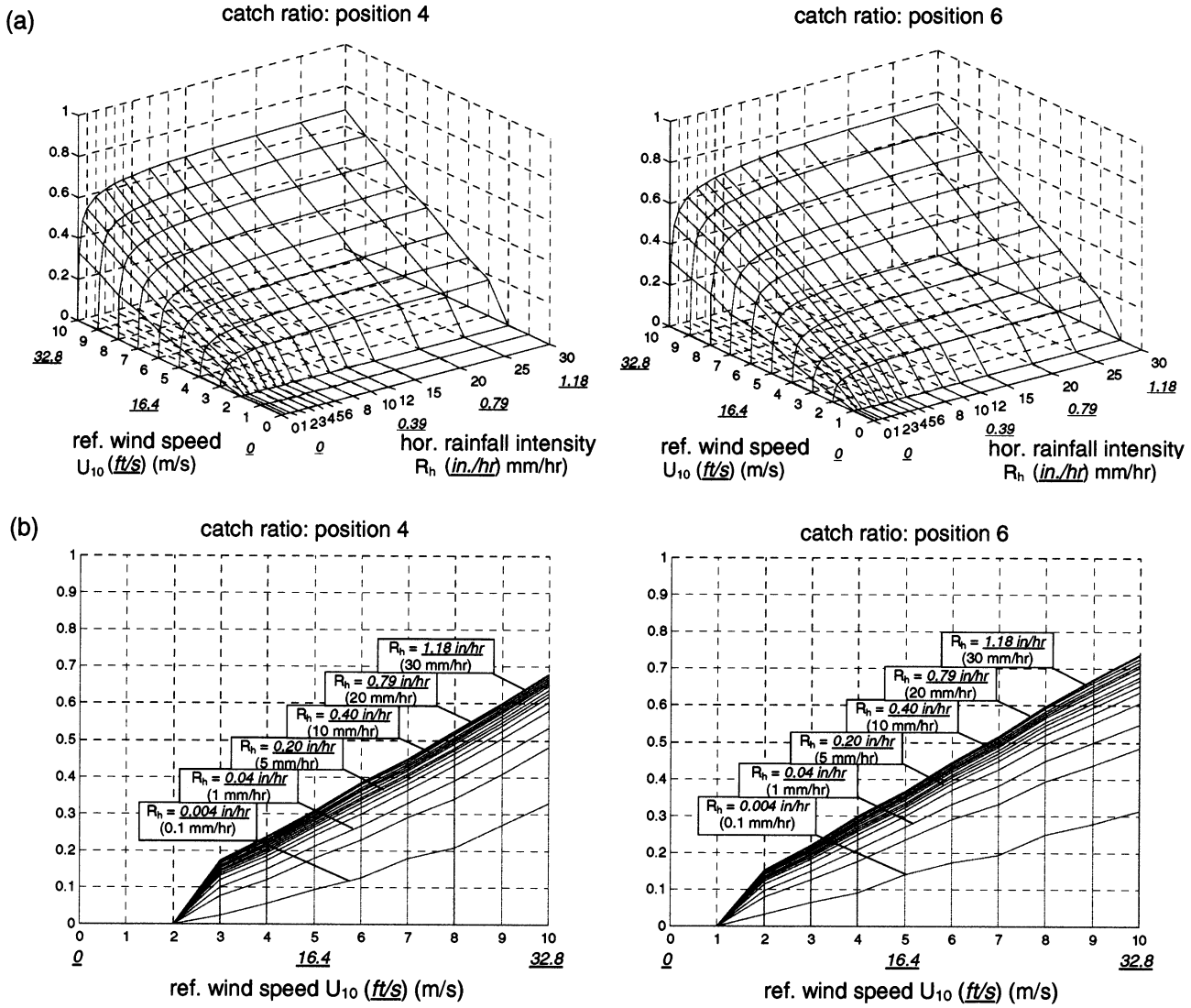

Figure 6 *Catch ratio (numerical) as a function of wind speed* U_{10} *and rainfall intensity* R_h *for position 4 (left figure) and position 6 (right figure) at the southwest facade. (a) Three-dimensional plot and (b) two-dimensional plot with rainfall intensity as a parameter.*

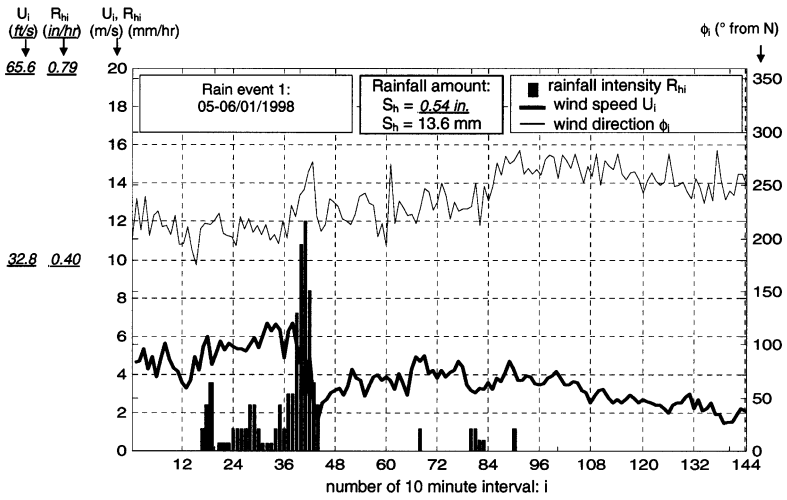

Figure 7 *Measurements of wind speed* U_i*, wind direction* φ_i*, and rainfall intensity* R_{hi} *for each 10-minute interval* i *in the one-day rain event (January 5 and 6, 1998). Total horizontal rainfall amount: 0.54 in. (13.6 mm).*

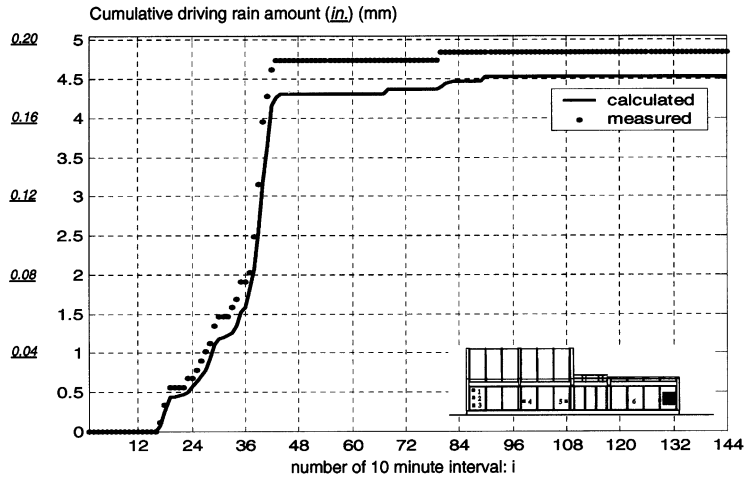

Figure 8 *Temporal distribution of the experimentally and numerically determined cumulative driving rain amount during the rain event at gauge position 7.*

multiples of 0.0044 in. (0.113 mm) could be measured and presented in the cumulative plot.

Spatial Distribution of Driving Rain

When employing the same numerical procedure for all 40320 zones of the southwest facade, and not focusing on the temporal distribution but only on the cumulative driving rain amount at the end of the rain event, contours for the catch ratio are obtained (Figure 9a). In addition, the numerical catch ratio values at the driving rain gauge positions are given. The catch ratio values at the end of the rain event are to be multiplied with the total horizontal rainfall amount S_h = 0.54 in. (S_h = 13.6 mm) to obtain the corresponding driving rain amount. The measurement error for the catch ratio values is about 0.02.

A distinct wetting pattern is found. Approximately the same observations as before are made—sweeping effect causing highest values near the vertical and roof edges, higher values for the flat roof module, etc. It is noted that the abrupt transition (shelter line) between sheltered and nonsheltered

areas has disappeared, and that the highest catch ratio values are no longer situated just below the sheltered area but somewhere lower on the facade. The reason is twofold: (1) the presence of raindrops of different diameters in the rain event, all with a shelter line at a slightly different location, and (2) the fluctuations in wind speed during the rain event, causing the shelter line for each of the raindrop diameters to move vertically across the facade as a function of time. Comparing the numerical results with the measurement values in Figure 9b, a good agreement is obtained (remark: the value in the middle of the facade was not measured). Some discrepancies are observed at the edges, especially at gauge positions 1 and 2. These are the most difficult positions to predict due to the presence of both the sweeping effect (upward and sideward) and the shelter effect at these positions. Moreover, position 1 is situated exactly on the transition region between the sheltered and nonsheltered area where a high wetting gradient is present (Figure 9a).

Finally, it is stressed that the numerical catch ratio values displayed in Figure 9a were obtained based on 10-minute measurements of wind speed and rainfall intensity (Figure 7). It is also possible to use hourly or daily averaged values of wind speed and rainfall intensity as input for the numerical method. Special attention, however, is required since using low-frequency data can introduce significant errors, as will be shown in the next section.

TIME REPRESENTATIVENESS OF CLIMATIC INPUT DATA

In this section, the influence of time averaging of the input data for the numerical method (wind speed, rainfall intensity) on the accuracy of the result (driving rain amount) is addressed. Let us recall Figure 1, giving the catch ratio for a certain position on the building envelope and for a certain wind direction. In the numerical method for transient rain events, the catch ratio for each time step is obtained by using the wind speed and rainfall intensity value for this time step as input in the surface plot (Figure 1) (e.g., using a time step of 10 minutes, the 10-minute wind speed and rainfall intensity values used yield the 10-minute catch ratio value [driving rain amount]). Summing the 10-minute driving rain amounts yields the total amount of driving rain for a certain time period. The same procedure can be followed using hourly or daily values of wind speed and rainfall intensity as input in the surface plots, yielding hourly or daily catch ratio (driving rain amount) values that, again, are summed to obtained the total driving rain amount.

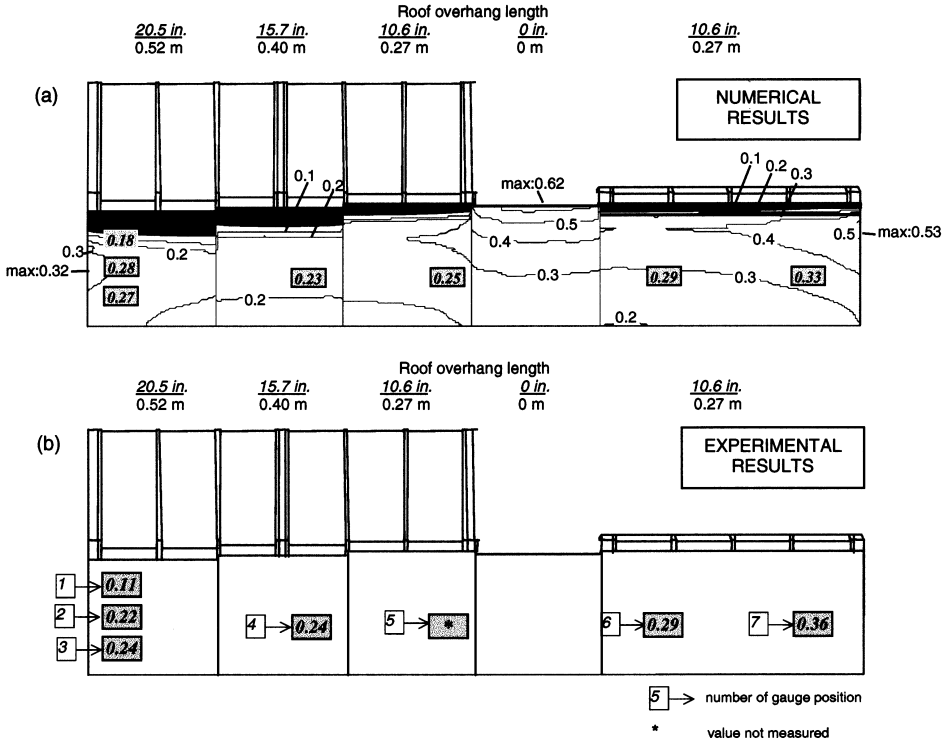

Figure 9 *(a) Contours (numerical) illustrating the spatial distribution of the catch ratio at the end of the rain event. The numerical catch ratio values at the positions of the driving rain gauges are additionally indicated. (b) Experimental results for the spatial distribution of the catch ratio.*

Ideally, using 10-minute, hourly, or daily time steps should give the same summed driving rain amount for a fixed period of time. However, data averaging inevitably leads to a loss of accuracy. Whether the numerical prediction will be successful or not depends to a large extent on the size of this time step and the way in which the data values for this time step are obtained. The natural fluctuations of wind and rain characteristics suggest that measurement samples should be gathered for sufficiently small time steps in order to be representative (i.e., to yield a good estimate of the corresponding driving rain load). In the previous sections, the use of 10-minute data was positively evaluated. However, the current standards BS 8104 (BSI 1992) and PrEN 13013-3 (CEN 1997) and other simplified calculation methods (Sanders 1996) for driving rain request, at best, hourly averaged data. In practice, daily values are often used. Most databases also consist of daily values. These values are usually obtained from averaging 10-minute measurement data. The averaging technique that is generally used and agreed upon is arithmetic averaging. The question arises as to whether or not the loss of accuracy by arithmetic averaging over a long period compromises the time representativeness of the data and, if so, whether a better averaging technique can be derived.

Blocken and Carmeliet (2000b) have demonstrated that errors introduced by arithmetic averaging of 10-minute wind speed and rainfall intensity data over an hour or a day can give rise to large errors in the resulting driving rain amounts, going up to 40% and 80%, respectively. A weighted averaging technique was derived to transform values of wind speed and rainfall intensity at a small time scale (index i; size, e.g., 10 minutes) into averaged values at a larger time scale (index j; size, e.g., 1 hour, 1 day,...) without abandoning time representativeness.

$$U_j = \frac{\sum_i U_i S_{hi}}{\sum_i S_{hi}}, \; R_{hj} = \frac{\sum_i R_{hi} S_{hi}}{\sum_i S_{hi}} \qquad (4)$$

where the sum extends over all time steps *i* in time step *j* and where

U_i = wind speed value for time step *i* (small time scale),

S_{hi} = rainfall amount value for time step *i* (small time scale),

R_{hi} = rainfall intensity value for time step *i* (small time scale),

U_j and R_{hj} = weighted averaged wind speed/rainfall intensity values for time step *j* (large time scale).

The weighted averaging technique accentuates the joint occurrence of wind and rain (by weighting the wind speed values with the corresponding rainfall amounts) and compensates for peak suppression in the averaging procedure. These are the aspects that are failed by the commonly used averaging techniques.

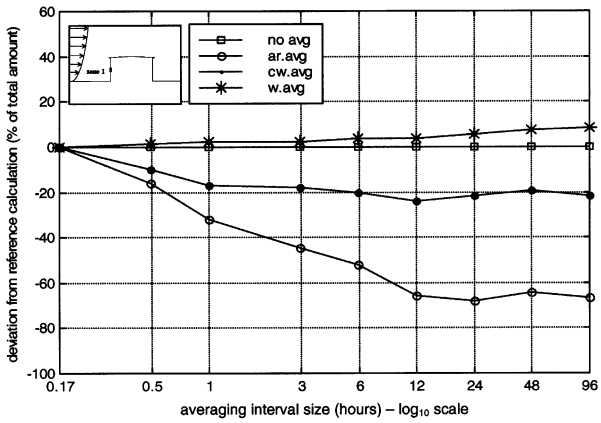

Figure 10 *The errors (%) introduced by the use of different averaging techniques for wind and rain data to calculate the total driving rain load. Errors are displayed as a function of the averaging interval size (*no avg = *without averaging, using ten-minute values of wind speed and rainfall intensity;* ar. avg = *arithmetic averaging;* cw. avg = *crude weighted averaging;* w. avg = *weighted averaging).*

The performance of the weighted averaging technique as opposed to these other techniques is illustrated in Figure 10, giving results from an exploratory study (Blocken and Carmeliet 2000b). The error introduced by calculating the driving rain amount on a zone of a low-rise building based on averaged values of wind speed and rainfall intensity is displayed as a function of the averaging interval size. The averaged wind and rain data values are obtained by averaging 10-minute values. The error is calculated as the percentage deviation from the reference solution (reference = total driving rain amount calculated directly from the 10-minute input data without averaging):

$$e = 100 \cdot \frac{S^n_{dr\_AVG} - S^n_{dr\_REF}}{S^n_{dr\_REF}} \; (\%) \qquad (5)$$

where

$S_{dr}{}^n{}_{\_AVG}$ = driving rain amount obtained based on the averaged data,

$S_{dr}{}^n{}_{\_REF}$ = reference solution,

The averaging techniques studied are arithmetic averaging (summing values and dividing sum by the number of terms), crude weighted averaging (same, but only averaging during rain—this technique is rather exceptionally used as an alternative for arithmetic averaging), and weighted averaging. The main observation is the important underestimation error caused by the arithmetic and crude weighted averaging techniques, even when averaging on an hourly basis—the time step that is generally used and agreed upon—and the good

performance of the weighted averaging technique at this time scale. For more details, the reader is referred to Blocken and Carmeliet (2000b).

DISCUSSION AND CONCLUSIONS

1. A three-dimensional numerical method has been employed to determine the spatial and temporal distribution of driving rain on a low-rise building of complex geometry for a recorded rain event.
2. Distinct wetting patterns have been found. The following three particular causes for these patterns have been identified: (1) sweeping of raindrops toward vertical building edges, (2) sweeping of raindrops toward top edges, and (3) shelter effect by various roof overhang configurations. Consequently, the building facade positions that receive the largest amounts of driving rain are the top edges (when no roof overhang is present) and side edges. When roof overhang is present, the largest amounts occur somewhere below the sheltered area, where a high-wetting gradient is present. In general, the driving rain amounts strongly increase with increasing wind speed. The influence of rainfall intensity has appeared to be rather small.
3. The experimental verification has shown the capability of accurately determining both the spatial and temporal distribution of driving rain with the current method.
4. Special care must be given to time representativeness of the climatic input data (wind speed, wind direction, rainfall intensity) for the numerical method. Using arithmetically hourly or daily averaged data can yield large errors in resulting driving rain amounts, indicating that both the current standards and most of the current climatic databases might not be accurate enough for driving rain estimation. One should consider building databases including either high-frequency data (e.g., 1/600 Hz) or averaged data (hourly, daily,...) calculated from high-frequency data using the weighted averaging technique.

The important assumptions adopted for the present study are:

- The raindrop size distribution according to Best (1950). Although this formula is based on an extensive study for a large number of rain events, deviations from the prescribed spectra can occur. It was briefly indicated here that the sensitivity to raindrop spectra might be rather small (as was also suggested in the work of Choi (1994b)). Further research is required to verify this.
- The turbulent dispersion of raindrops was neglected. Although frequently accounted for in the past, the experimental verification performed here and in an earlier paper (Blocken and Carmeliet 2000a) has illustrated that, in the building situation under study, accurate results can be obtained without modeling turbulent dispersion.

ACKNOWLEDGMENTS

This research is funded by the Government of Flanders (Belgium). As a Flemish Government institution, IWT (Vlaams Instituut voor de Bevordering van het Wetenschappelijk-Technologisch Onderzoek in de Industrie) supports and stimulates industrial research and technology transfer in the Flemish Industry. Their contribution is gratefully acknowledged.

REFERENCES

Best, A.C. 1950. The size distribution of raindrops. *Quarterly Journal of the Royal Meteorological Society* 76: pp. 16-36.

Blocken, B., and J. Carmeliet. 2000a. Driving rain on building envelopes I, numerical estimation and full-scale experimental verification. *Journal of Thermal Envelope and Building Science* 24 (1): 61-85.

Blocken, B., and J. Carmeliet. 2000b. Driving rain on building envelopes II, representative experimental data for driving rain estimation. *Journal of Thermal Envelope and Building Science* 24 (2): 89-110.

Blocken, B., H. Hens, and J. Carmeliet. 2001. *Methods for the quantification of driving rain on buildings*. Submitted for presentation at the ASHRAE Winter Meeting, January 12-16, Atlantic City, NJ.

Bollen, S., and G. Eerdekens. 1998. Regenbelasting van gevels (driving rain on building facades). Master's thesis, Laboratory of Building Physics, Katholieke Universiteit Leuven (in Dutch).

BSI. 1992. *BS 8104*. Code of practice for assessing exposure of walls to wind-driven rain.

CEN. 1997. *PrEN 13013-3, Hygrothermal performance of buildings—Climatic data, part 3: Calculation of a driving rain index for vertical surfaces from hourly wind and rain data*.

Choi, E.C.C. 1991. *Numerical simulation of wind-driven-rain falling onto a 2-D building*. Hong Kong: Asia Pacific Conference on Computational Mechanics, pp. 1721-1728.

Choi, E.C.C. 1993. Simulation of wind-driven-rain around a building. *Journal of Wind Engineering and Industrial Aerodynamics* 46 and 47: 721-729.

Choi, E.C.C. 1994a. Determination of wind-driven-rain intensity on building faces. *Journal of Wind Engineering and Industrial Aerodynamics* 51: 55-69.

Choi, E.C.C. 1994b. Parameters affecting the intensity of wind-driven rain on the front face of a building. *Journal of Wind Engineering and Industrial Aerodynamics* 53: 1-17.

Etyemezian, V., C.I. Davidson, M. Zufall, W. Dai, S. Finger, and M. Striegel. 2000. Impingement of raindrops on a tall building. *Atmospheric Environment* 34: 2399-2412.

Hangan, H. 1999. Wind-driven rain studies. A C-FD-E approach. *Journal of Wind Engineering and Industrial Aerodynamics* 81: 323-331.

Högberg, A.B., M.K. Kragh, and F.J.R. van Mook. 1999. A comparison of driving rain measurements with different gauges. *Proceedings of 5th Symposium on Building Physics in the Nordic Countries, Gothenburg*, pp. 361-368.

Lakehal, D., P.G. Mestayer, J.B. Edson, S. Anquetin,and J.-F. Sini. 1995. Eulero-Lagrangian simulation of raindrop trajectories and impacts with the urban canopy. *Atmospheric Environment* 29 (23): 3501-3517.

Karagiozis, A., and G. Hadjisophocleous. 1996. Wind-driven rain on high rise buildings. *Thermal Performance of the Exterior Envelopes of Buildings VI*. Atlanta: American Society of Heating, Refrigerating and Air-Conditioning Engineers, Inc.

Karagiozis, A., G. Hadjisophocleous, and S. Cao. 1997. Wind-driven rain distributions on two buildings. *Journal of Wind Engineering and Industrial Aerodynamics* 67 and 68: 559-572.

Kim, S.-E., D. Choudhury, and B. Patel. 1997. Computations of complex turbulent flows using the commercial code FLUENT. *Proceedings of the ICASE/LaRC/AFOSR Symposium on Modeling Complex Turbulent Flows*, Hampton, Virginia.

Kragh, M.K. 1998. *Microclimatic conditions at the external surface of building envelopes*, Ph.D. thesis, Technical University of Denmark, Department of Buildings and Energy, Report R-027.

Sanders, C. 1996. *Heat, air and moisture transfer in insulated envelope parts, Final report, Volume 2, Task: 2: Environmental conditions*. Acco, Leuven: International Energy Agency Annex 24.

Sankaran, R., and D.A. Paterson. 1995. Computation of rain falling on a tall rectangular building. *Proceedings of 9ICWE*, New Delhi, India.

Shih, T.-H., W.W. Liou, A. Shabbir, and J. Zhu. 1995. A new k-ε eddy-viscosity model for high Reynolds number turbulent flows—Model development and validation. *Computers and Fluids* 24 (3): 227-238.

Van Mook, F.J.R., M.H. De Wit, and J.A. Wisse. 1997. Computer simulation of driving rain on building envelopes. *Proceedings of 2EACWE*, Genova, Italy, pp. 1059-1066.

Van Mook, F.J.R. 1998. *Measurements of driving rain by a driving-rain gauge with a wiper*. CIB taskgroup 21 meeting, Gävle, Sweden.

Van Mook, F.J.R. 1999a. Full-scale measurements and numeric simulations of driving rain. *Proceedings of 10 ICWE*, Copenhagen, Denmark, pp. 1145-1152.

Van Mook, F.J.R. 1999b. Measurements and simulations of driving rain on the main building of the TUE. *Proceedings of 5th Symposium on Building Physics in the Nordic Countries*, Gothenburg, Sweden, pp. 377-384.

Wisse, J.A. 1994. Driving rain, a numerical study. *Proceedings of 9th Symposium on Building Physics and Building Climatology*, Dresden, September.